Molecular dynamics study on the equilibrium magnetization properties and structure of ferrofluids

Zuowei Wang,* Christian Holm,† and Hanns Walter Müller‡
Max-Planck-Institut für Polymerforschung, Ackermannweg 10, D-55128 Mainz, Germany
(Received 21 March 2002; published 21 August 2002)

We investigate in detail the initial susceptibility, magnetization curves, and microstructure of ferrofluids in various concentration and particle dipole moment ranges by means of molecular dynamics simulations. We use the Ewald summation for the long-range dipolar interactions, take explicitly into account the translational and rotational degrees of freedom, coupled to a Langevin thermostat. When the dipolar interaction energy is comparable with the thermal energy, the simulation results on the magnetization properties agree with the theoretical predictions very well. For stronger dipolar couplings, however, we find systematic deviations from the theoretical curves. We analyze in detail the observed microstructure of the fluids under different conditions. The formation of clusters is found to enhance the magnetization at weak fields and thus leads to a larger initial susceptibility. The influence of the particle aggregation is isolated by studying ferro-solids, which consist of magnetic dipoles frozen in at random locations but which are free to rotate. Due to the artificial suppression of clusters in ferrosolids the observed susceptibility is considerably lowered when compared to ferrofluids.

DOI: 10.1103/PhysRevE.66.021405 PACS number(s): 61.20.Ja, 75.50.Mm, 82.70.Dd, 82.20.Wt

I. INTRODUCTION

Ferrofluids (dipolar magnetic fluids) are colloidal suspensions of ferromagnetic particles of about 10 nm diameter dispersed in a carrier liquid [1] that are usually stabilized against agglomeration by coating particles with long-chain molecules (sterically) or decorating them with charged groups (electrostatically). The small size of the particles favors magnetic mono-domains with a magnetic moment proportional to the volume of the magnetic grains. As a result, the particles interact with each other by the long-range anisotropic dipole-dipole potential as well as the short-range symmetric potentials, such as the steric repulsion, the electrostatic repulsion, and the van der Waals attraction. The study of both the magnetization properties and structure of ferrofluids are of both fundamental and application interests.

A ferrofluid system of sufficiently low concentration behaves like an ideal paramagnetic gas. The interactions between the particles can be neglected, and the physical properties of the system are well described by the one-particle model [2]. In this case, the equilibrium magnetization is written in terms of the Langevin function $\mathcal{L}(\alpha)=\coth(\alpha)-1/\alpha$,

$$M_L = M_{sat}\mathcal{L}(\alpha), \quad M_{sat}=\frac{N}{V}\frac{m}{\mu_0}. \tag{1}$$

Here, M_{sat} is the saturation magnetization of the fluid, $\alpha = mH/kT$ is the Langevin parameter, and m is the magnetic moment, N/V denotes the number density of the particles, H is the magnetic field, T the temperature, k the Boltzmann constant, and $\mu_0 = 4\pi\times 10^{-7}$ H/m. Equation (1) leads to Curie's law for the initial susceptibility χ_L that depends linearly on the particle concentration,

$$\chi_L = \frac{N}{V}\frac{m^2}{3\mu_0 kT}. \tag{2}$$

However, experiments on concentrated ferrofluids have revealed an essential deviation from the Langevin formula [3]. The initial susceptibility increases with the particle concentration much faster than that predicted in Eq. (2). This deviation is clearly due to the particle interactions.

The influence of the particle interactions on the physical properties of ferrofluids is investigated in terms of two dimensionless parameters. One is the volume fraction of the particles,

$$\phi = \frac{N}{V}\frac{\pi\sigma^3}{6}, \tag{3}$$

with σ the particle diameter. The other is the dipolar coupling constant

$$\lambda = \frac{m^2}{4\pi\mu_0 kT\sigma^3}, \tag{4}$$

which relates the dipole-dipole interaction energy of two contacting particles to the thermal energy kT. The two parameters can be combined into the Langevin initial susceptibility χ_L in Eq. (2) as $\chi_L = 8\phi\lambda$.

A number of theoretical models allow the evaluation of the equilibrium magnetization of ferrofluids [4–13]. Among them, the mean-spherical model [6,7], the thermodynamic perturbation model [8], and the modified variant of the effective field model [9] have been shown to give good results for the magnetic properties of ferrofluids with low or moderate concentration of magnetic particles (up to 10–12 %). Taking χ_L as a universal parameter in weak magnetic fields, all the above approaches lead to the same expression for the initial susceptibility,

$$\chi = \chi_L(1+\chi_L/3). \tag{5}$$

*Electronic address: wangzuo@mpip-mainz.mpg.de
†Electronic address: holm@mpip-mainz.mpg.de
‡Electronic address: hwm@mpip-mainz.mpg.de

For ferrofluids of higher concentration, larger particle size, or at low temperature, Eq. (5) is insufficient [10]. Higher-order corrections in the dependence of χ or M on ϕ, λ, or in general on χ_L, turn out to be crucial.

An expression for χ up to cubic accuracy in χ_L can be obtained by the mean-spherical model [6], the Born-Mayer expansion method [11], and the statistical model based on the pair correlation function [10], which reads as [10]

$$\chi = \chi_L(1+\chi_L/3+\chi_L^2/144). \tag{6}$$

The cubic term makes a noticeable difference of 5% over Eq. (5) for $\chi_L \geqslant 4.14$. The significance of the third-order contribution has been verified in comparison with experimental measurements on the temperature dependence of χ [10]. However, in what we classify here as the strong coupling limit, $\lambda > 2$, the enhanced particle aggregation is not sufficiently accounted for by the analytical studies, thus giving rise to considerable deviations from the predictions of Eqs. (5) and (6). Here the magnetic properties turn out to depend on Φ and λ separately rather than χ_L alone, a point which we will try to elucidate with our simulation study.

Previous simulation works on dipolar (ferro)fluids were mainly undertaken to explore the phase diagram. Large ranges of particle concentration and dipolar coupling strength have been examined. The results are found to depend substantially on the employed short-range interactions, such as hard sphere [14–17], soft sphere [18–21], and Lennard-Jones (LJ) potentials [22,23]. As an example, the question whether a minimum amount of dispersive energy, i.e., the attractive van der Waals energy, is required to observe the liquid-vapor coexistence is still under discussion [17,20–25]. Recent studies on the magnetic properties include the Monte Carlo simulations on the dispersions of interacting superparamagnetic particles in a solid matrix [26] and on ferrofluids with a finite spherical boundary [27]. In order to compare with the macroscopic theories on ferrofluids, it is necessary to simulate the ferrofluid systems with truly periodic boundary conditions.

In this paper, the Langevin dynamics simulation method is used to study the equilibrium properties of ferrofluids. The long-range dipolar interactions are dealt with the Ewald summation. The initial susceptibility and the magnetization curves are calculated as a function of ϕ and λ. The simulation results are directly compared with the theoretical models. The influence of particle aggregation is investigated systematically by performing a cluster analysis of the microstructure of the systems. The formation of aggregates is found to enhance the magnetization of ferrofluids at weak magnetic fields. This is confirmed by comparison with the calculated initial susceptibility for a ferrosolid, i.e., a ferrofluid with the same properties but with the particles' translational degree of freedom frozen in at random positions.

The paper is organized as follows. We describe the simulation method in Sec. II. The simulation results on the initial susceptibility and the magnetization curves are given in Secs. III A and B, respectively. The cluster analysis of the microstructure is presented in Sec. III C. The initial susceptibility of the ferrosolid systems is calculated in Sec. III D. We end with our conclusions in Sec. IV.

II. SIMULATION METHOD

The investigated ferrofluid systems consist of N spherical particles of diameter σ distributed in a cubic simulation box of side length L. Each particle has a permanent point dipole moment $\mathbf{m_i}$ at its center. Using periodic boundary conditions in all spatial directions, the dipole-dipole interaction potential between particle i and j is given by

$$U_{ij}^{dip} = \frac{1}{4\pi\mu_0} \sum_{\mathbf{n}\in\mathbf{Z}^3} \left\{ \frac{\mathbf{m}_i\cdot\mathbf{m}_j}{|\mathbf{r}_{ij}+\mathbf{n}L|^3} - \frac{3[\mathbf{m}_i\cdot(\mathbf{r}_{ij}+\mathbf{n}L)][\mathbf{m}_j\cdot(\mathbf{r}_{ij}+\mathbf{n}L)]}{|\mathbf{r}_{ij}+\mathbf{n}L|^5} \right\}, \tag{7}$$

where $\mathbf{r}_{ij}=\mathbf{r}_i-\mathbf{r}_j$ is the displacement vector of the two particles. The sum extends over all simple cubic lattice points, $\mathbf{n}=(n_x,n_y,n_z)$ with n_x, n_y, n_z integers.

In this work, we use the Ewald summation for dipolar systems to evaluate Eq. (7) effectively, which gives [28–30]

$$U_{ij}^{dip} = U_{ij}^{(r)} + U_{ij}^{(k)} + U_{ij}^{(self)} + U_{ij}^{(surf)}, \tag{8}$$

where the real-space $U_{ij}^{(r)}$, the k space (reciprocal space) $U_{ij}^{(k)}$, the self $U_{ij}^{(self)}$, and the surface $U_{ij}^{(surf)}$ contributions are respectively given by

$$U_{ij}^{(r)} = \frac{1}{4\pi\mu_0} \sum_{\mathbf{n}\in\mathbf{Z}^3} \{(\mathbf{m}_i\cdot\mathbf{m}_j)B(|\mathbf{r}_{ij}+\mathbf{n}|) - [\mathbf{m}_i\cdot(\mathbf{r}_{ij}+\mathbf{n})] \times [\mathbf{m}_j\cdot(\mathbf{r}_{ij}+\mathbf{n})]C(|\mathbf{r}_{ij}+\mathbf{n}|)\}, \tag{9}$$

$$U_{ij}^{(k)} = \frac{1}{4\pi\mu_0 L^3} \sum_{\mathbf{k}\in\mathbf{Z}^3,\mathbf{k}\neq 0} \frac{4\pi}{k^2} \exp[-(\pi k/\kappa L)^2](\mathbf{m}_i\cdot\mathbf{k}) \times (\mathbf{m}_j\cdot\mathbf{k}) \exp(2\pi i\mathbf{k}\cdot\mathbf{r}_{ij}/L), \tag{10}$$

$$U_{ij}^{(self)} = -\frac{1}{4\pi\mu_0}\frac{2\kappa^3}{3\sqrt{\pi}}(m_i^2+m_j^2), \tag{11}$$

$$U_{ij}^{(surf)} = \frac{1}{4\pi\mu_0}\frac{4\pi}{(2\mu_{BC}+1)L^3}\mathbf{m}_i\cdot\mathbf{m}_j \tag{12}$$

with

$$B(r) = [\mathrm{erfc}(\kappa r) + (2\kappa r/\sqrt{\pi})\exp(-\kappa^2 r^2)]/r^3, \tag{13}$$

$$C(r) = [3\,\mathrm{erfc}(\kappa r) + (2\kappa r/\sqrt{\pi})(3+2\kappa^2 r^2) \times \exp(-\kappa^2 r^2)]/r^5. \tag{14}$$

Here $\mathrm{erfc}(x) := 2\pi^{-1/2}\int_x^\infty \exp(-t^2)\mathrm{d}t$ denotes the complementary error function. The inverse length κ is the splitting parameter of the Ewald summation. Equation (12) assumes that the set of the periodic replications of the simulation box

tends in a spherical way towards an infinite cluster and that the medium outside this sphere is a uniform medium with magnetic permeability μ_{BC}. In this work, we use the metallic boundary condition $\mu_{BC}=\infty$. The surface term vanishes in this case and demagnetization effects do not occur. Thus, the applied external magnetic field **H** coincides exactly with the internal field. The influence of different boundary conditions on the simulation results will be the topic of a subsequent publication [31]. The related formulas for the dipolar forces and torques can be found in a previous paper [30]. The theoretical estimates of the cutoff errors in the Ewald summation derived there are used to determine the optimal values for the Ewald parameters which enable us to minimize the overall computational time at a predefined accuracy.

The short-range interaction potential between the particles is chosen to mimic the steric mechanism for stabilizing the colloidal suspension. As mentioned in Sec. I, it is still not settled which kind of potential is most suitable to model real ferrofluids. It might actually depend on whether the solution is electrically or sterically stabilized. In this work we adopt the Lennard-Jones potential

$$U_{ij}^{LJ}=4\varepsilon\left[\left(\frac{\sigma}{r_{ij}}\right)^{12}-\left(\frac{\sigma}{r_{ij}}\right)^{6}-C(R_c)\right], \tag{15}$$

where $C(R_c)=(\sigma/R_c)^{12}-(\sigma/R_c)^6$ with a cutoff radius of $R_c=2^{1/6}\sigma$. In this way the particles have a purely repulsive interaction force that smoothly decays to zero at R_c. This cutoff range is smaller than the one usually used in the soft sphere potential which is commonly adopted as $U_{SS}(r_{ij})=4\varepsilon(\sigma/r_{ij})^{12}$ [18–21], and thus closer to the hard sphere potential as employed in most other theoretical calculations [10,11]. In this context the analytical calculations of Ivanov [10] reveal that at least for the spatially homogeneous systems the influence of different short-range repulsive potentials seems to be marginal.

The translational and rotational Langevin equations of motion of particle i are given by [29,32]

$$\mathcal{M}_i\dot{\mathbf{v}}_i=\mathbf{F}_i-\Gamma_T\mathbf{v}_i+\boldsymbol{\xi}_i^T, \tag{16}$$

$$\mathbf{I}_i\cdot\dot{\boldsymbol{\omega}}_i=\boldsymbol{\tau}_i-\Gamma_R\boldsymbol{\omega}_i+\boldsymbol{\xi}_i^R, \tag{17}$$

where $\mathcal{M}_i$ and $\mathbf{I}_i$ are the mass and inertia tensor of the particle, Γ_T and Γ_R are the translational and rotational friction constants, respectively. The Gaussian random force and torque have the properties that the first moments vanish,

$$\langle\xi_{i\alpha}^T(t)\rangle=0, \tag{18}$$

$$\langle\xi_{i\alpha}^R(t)\rangle=0, \tag{19}$$

while the second moments satisfy

$$\langle\boldsymbol{\xi}_{i\alpha}^T(t)\cdot\boldsymbol{\xi}_{j\beta}^T(t')\rangle=6kT\Gamma_T\delta_{ij}\delta_{\alpha\beta}\delta(t-t'), \tag{20}$$

$$\langle\boldsymbol{\xi}_{i\alpha}^R(t)\cdot\boldsymbol{\xi}_{j\beta}^R(t')\rangle=6kT\Gamma_R\delta_{ij}\delta_{\alpha\beta}\delta(t-t'), \tag{21}$$

where α and β denote the x,y,z components in the Cartesian coordinates, respectively. Introducing the dipolar and short-range terms into Eqs. (16) and (17), the dimensionless equations of motion can now be written as

$$\dot{\mathbf{v}}_i^*=\sum_{j\neq i}(\mathbf{F}_{ij}^{dip*}+\mathbf{F}_{ij}^{LJ*})-\Gamma_T^*\mathbf{v}_i^*+\boldsymbol{\xi}_i^{T*}, \tag{22}$$

$$\mathbf{I}_i^*\cdot\dot{\boldsymbol{\omega}}_i^*=\sum_{j\neq i}\boldsymbol{\tau}_{ij}^{dip*}+\mathbf{m}_i^*\times\mathbf{H}^*-\Gamma_R^*\boldsymbol{\omega}_i^*+\boldsymbol{\xi}_i^{R*}, \tag{23}$$

where the variables are given in dimensionless form reduced by the following units: length $r^*=r/\sigma$, dipole moment $m^{*2}=m^2/4\pi\mu_0\epsilon\sigma^3$, moment of inertia $I^*=I/(\mathcal{M}\sigma^2)$, time $t^*=t(\epsilon/\mathcal{M}\sigma^2)^{1/2}$, the friction constants $\Gamma_T^*=\Gamma_T(\sigma^2/\mathcal{M}\epsilon)^{1/2}$, and $\Gamma_R^*=\Gamma_R/(\mathcal{M}\sigma^2\epsilon)^{1/2}$, magnetic field $H^*=H(4\pi\mu_0\sigma^3/\epsilon)^{1/2}$ as well as temperature $T^*=kT/\epsilon$. The values of the dimensionless friction constants do not affect the equilibrium properties. Here we adopt $\Gamma_T^*=10.0$ and $\Gamma_R^*=3.0$, because in our simulations these values had been found to speed up the equilibration time. These values are also close to that used in Ref. [32]. A value of $I^*=0.4$ is used for the dimensionless moment of inertia, corresponding to that of a rigid sphere with diameter σ.

The simulations were performed at constant temperature $T^*=1$. The orientational coordinates of the particles were expressed in terms of quaternion parameters and the equations of motions were integrated with a leap-frog algorithm [29]. A reduced time step $\Delta t^*=0.002$ was employed in all simulations. The runs were started from initial configurations with random particle positions and dipole moment orientations. For each case, the system was at first equilibrated for a period of 50 000 time steps. The magnetization and structural properties were then calculated from the data for another period of at least 200 000 time steps. Error bars for the simulation results were determined by dividing the simulation runs into blocks of 10 000 time steps and calculating an estimate for the standard deviation of the mean [33].

III. RESULTS AND DISCUSSION

Results were obtained from simulations on systems with $N=1000$ particles. The number density of the particles was mostly taken in the range of $\rho^*=N/V^*\leqslant 0.45$, corresponding to volume fractions $\phi=\rho^*\pi/6\leqslant 0.236$. This covers the typical particle concentration ranges which are obtainable in real ferrofluids. A few more runs were also carried out at higher concentrations in case of smaller λ in order to reach a sufficiently large χ_L. The values of the dipolar coupling constant λ were mainly chosen to be 1,2,3, and 4. To get an estimate of realistic λ values, we consider a ferrofluid sample consisting of monodispersed magnetite particles. The bulk magnetization of this material is $M_d=4.46\times10^5$ A/m. With a magnetic core diameter of the particles of $\sigma=10$ nm, the value of λ amounts to about 1.3 at room temperature $T=300$ K. For larger particles with $\sigma=13$ nm, λ rises up to 2.9 under the same conditions. Note that λ may further be enlarged by decreasing the temperature or using cobalt as working material ($M_d=14.01\times10^5$ A/m), for which the previous λ values increase by a factor of around

3.14. We therefore also carried out some simulations for $\lambda = 8$.

In all simulations, we fixed the root mean square (rms) absolute errors in the dipolar forces to $\Delta F^{dip} \leqslant 10^{-4} m^2/4\pi\mu_0\sigma^4$, which corresponds to $10^{-4}/6$ of the attractive force between two contacting particles with dipole moments in parallel alignment. The optimal values of the Ewald parameters had been determined separately for each system [30]. As an example, for a sample with $\rho^* = 0.1$ we get $r_c = 0.425L$, $\kappa = 6.78/L$, and $K_c = 6 \times 2\pi/L$. While $\rho^* = 0.3$ yields $r_c = 0.46L$, $\kappa = 6.84/L$, and $K_c = 7 \times 2\pi/L$ to be the optimum values, respectively.

A. Initial susceptibility

The influence of the particle interactions on the magnetic properties is most evident at weak fields, so we start with the investigation of the initial susceptibility χ. The value of χ is determined from the linear relationship of $\mathbf{M} = \chi\mathbf{H}$ at $H \to 0$. Simulations are thus performed to get the $M(H)$ curves at weak fields. The equilibrium magnetization $\mathbf{M}$ is evaluated by the prescription

$$\mathbf{M} = \frac{1}{\tau}\int_{t_0}^{t_0+\tau}\left(\frac{1}{\mu_0 V}\sum_{i=1}^{N}\mathbf{m}_i\right)dt, \tag{24}$$

where t_0 is the time needed for the system to establish the equilibrium state.

To study the weak field magnetization, we increase the Langevin parameter α from 0 to 0.5. As expected, the calculation of M at $\alpha = 0$ does not show the existence of a spontaneous magnetization, because ϕ is still not high enough. Other works [21] have shown that the transition to a ferromagnetic state occurs at $\phi \approx 0.44$ for $\lambda = 4$. For higher values of λ, the critical concentration is around $\phi \approx 0.35$ for $\lambda = 6.25$ [15,21] and $\phi \approx 0.31$ for $\lambda = 9$ [19]. These conditions are clearly not encountered in our simulations.

The dimensionless magnetization M^* $(= M/\sqrt{4\pi\epsilon/\mu_0\sigma^3})$ of the system with $\lambda = 3$ is shown in Fig. 1 as a function of α and ϕ. The results for other values of λ display a similar behavior. It can be seen that M^* at first increases linearly with α, then at higher field values sublinearly. We introduce α_{lin} as a definition for the maximum value of α where M^* still can be considered to obey the linear relationship. Evidently, at a fixed value of λ this α_{lin} value decreases with growing ϕ. The data in Fig. 1 show that when ϕ is increased from 0.052 to 0.209, α_{lin} decreases from 0.45 to about 0.25. On the other hand, at a fixed particle concentration, rising λ also implies a reduction of α_{lin}. This demonstrates that the range over which M is proportional to H (or equivalently α) shrinks with the increase of χ_L. For a quantitative evaluation of the initial susceptibility we need to determine the linear region for each case separately. This is accomplished with the help of a linear regression fit with error weighting [34]. The basic idea of that method is to minimize the so-called ξ-square merit function,

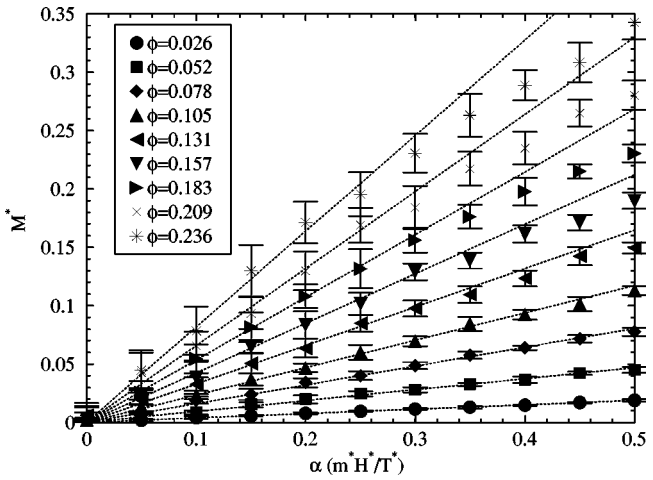

FIG. 1. Dimensionless magnetization M^* as a function of the Langevin parameter α and the volume fraction ϕ for a system with $\lambda = 3$. The symbols are the simulation results. The dashed curves are the linear fitting data, the slope of which gives the initial susceptibility χ.

TABLE I. Linear regression fitting results for the $M(H)$ $[M(\alpha)]$ curves in Fig. 1. The theoretical predictions of χ on different orders are also given for comparison.

ϕ	χ	$\Delta\chi$	$\xi^2/(N_{d,opt}-2)$	Q	$N_{d,opt}$	$\chi_L[Eq.\ (2)]$	$\chi[Eq.\ (5)]$	$\chi[Eq.\ (6)]$
0.0262	0.822	0.017	0.069	0.999	11	0.6283	0.7599	0.7616
0.0524	2.040	0.045	0.138	0.997	10	1.2566	1.7830	1.7968
0.0785	3.505	0.069	0.249	0.981	10	1.8849	3.0693	3.1158
0.1047	5.103	0.142	0.085	0.999	9	2.5133	4.6188	4.7290
0.1309	7.173	0.330	0.069	0.997	7	3.1416	6.4315	6.6468
0.1571	9.237	0.363	0.094	0.993	7	3.7699	8.5073	8.8794
0.1833	11.680	0.741	0.016	0.999	6	4.3982	10.8464	11.4372
0.2094	14.356	0.873	0.140	0.968	6	5.0266	13.4486	14.3306
0.2356	17.831	1.114	0.150	0.963	6	5.6549	16.3140	17.5698

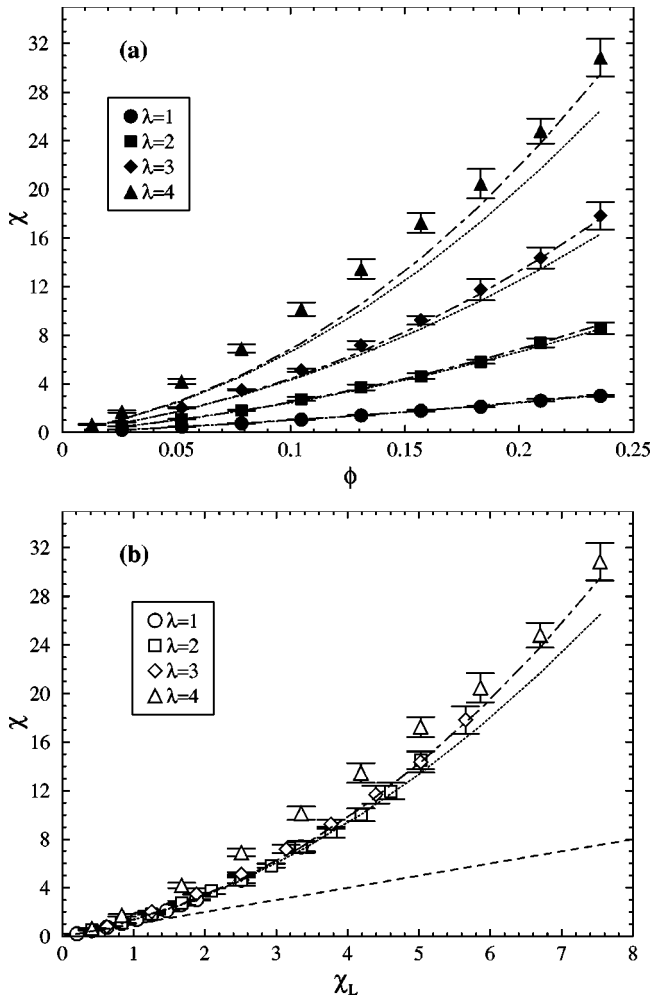

FIG. 2. (a) Initial susceptibility χ as a function of the dipolar coupling constant λ and volume fraction ϕ; (b) same data of χ as in (a), but mapped on the Langevin susceptibility χ_L. The theoretical curves are given by the Langevin model ($\chi=\chi_L$, dashed), Eq. (5) (dotted) and Eq. (6) (dot-dashed), respectively.

$$\xi^2=\sum_{i=1}^{N_d}\left(\frac{M_i-M(0)-\chi H_i}{\Delta M_i}\right)^2 \tag{25}$$

so as to get χ and its error bar. Here ΔM_i is the error bar related to the simulation data of M_i. In Fig. 1 the data were taken with a step size of $\Delta\alpha=0.05$ giving 11 data points on each curve. Since no spontaneous magnetization occurs, the initial data point is always at $M(0)=0.0$. For each curve, a series of linear fittings was generated by increasing N_d in Eq. (25) from 5 to 11. The fit which gives the minimum value of ξ^2 per degree of freedom is taken to be the optimum linear fitting to the data. The associated N_d-value is referred as $N_{d,opt}$. The slope χ and its error bar $\Delta\chi$ determine the initial susceptibility. The value of α_{lin} is roughly given by the product of $\Delta\alpha$ with $N_{d,opt}-1$. The results of this data fit including the error estimates are compiled in Table I. The degree of reliability of the results is reflected by the high goodness-probability Q [34]. The resulting straight lines $M=\chi H$, or in dimensionless form $M^*=\chi\alpha/4\pi\sqrt{\lambda/T^*}$, are also displayed in Fig. 1 to show how they fit to the simulation data.

Figure 2(a) shows the calculated initial susceptibility χ as a function of λ and ϕ, along with the analytical results from Eqs. (5) and (6). Since the Langevin susceptibility χ_L has been taken as the universal parameter in these theoretical predictions [8–10], we also map the data of χ on χ_L in Fig. 2(b) to show the scaling behavior more directly. In addition to the results in Fig. 2(a), some more data was produced at higher concentrations (up to $\phi=0.419$) for the case of $\lambda=1$ in order to get a larger range of χ_L. We did not combine such high concentrations with larger values of λ, since the close proximity to the magnetic phase separation would make the discussion more complex, rendering the results more sensitive to the specific short-range interaction.

For the weak interaction range $\lambda\leqslant 2$ we find perfect agreement with Eqs. (5) and (6) for all investigated volume fractions. Actually, because of these coupling parameters we can reach only up to $\chi_L<4$, both analytical predictions yield equally good results for our data and are indistinguishable within the error bars. For $\lambda=3$ we see small but significant deviations at low values of ϕ, meaning that already at low values of χ_L neither Eq. (5) nor Eq. (6) are accurate. However, at high volume fractions ($\chi_L>3$), the third-order Eq. (6) is compatible within error bars. For the numerical values of the data see Table I, where also the values of the analytical results for different orders are given for comparison. Even more drastic deviations from the theoretical predictions are found for $\lambda=4$ at low concentrations, in the range $\chi_L\leqslant 6$. We observe again the trend, that at higher volume fractions the third-order Eq. (6) becomes compatible with our data. We can conclude that the parameter λ, rather than χ_L, becomes the dominating control parameter for $\lambda>2$. This effect can be attributed directly to the microstructure formation in the system. When $\lambda\leqslant 2$, what we consider to be the weak interaction limit, the dipolar potential is comparable to the thermal fluctuation. Then the interparticle correlations are weak, and the present theoretical models work well. However, going to stronger interactions with $\lambda>2$, leads to a considerable amount of particle aggregation. The resulting clusters amplify the sensitivity of the system to weak external magnetic fields and thus lead to an enhanced magnetic susceptibility. We will come back to this point in Sec. III C.

The influence of the volume fraction seems to be weak in the investigated parameter regime. Noteworthy is that the third-order equation seems to describe the available data well at larger volume fraction and high coupling parameter λ, even better than it does at intermediate values. On the basis of our available data we cannot decide if this finding is a mere coincidence. To our knowledge, there is no theoretical reason to believe that the third-order equation should become reliable again at these high values of χ_L, where higher-order corrections of the form $\phi^m\lambda^n$ with m, n arbitrary, are expected to become important. Corrections linear in ϕ, but up to ninth order in λ have been assembled for the Born-Mayer expansion method in Ref. [11]. These additional terms are all positive and therefore necessarily increase the susceptibility. We have found that they improve the theoretical prediction

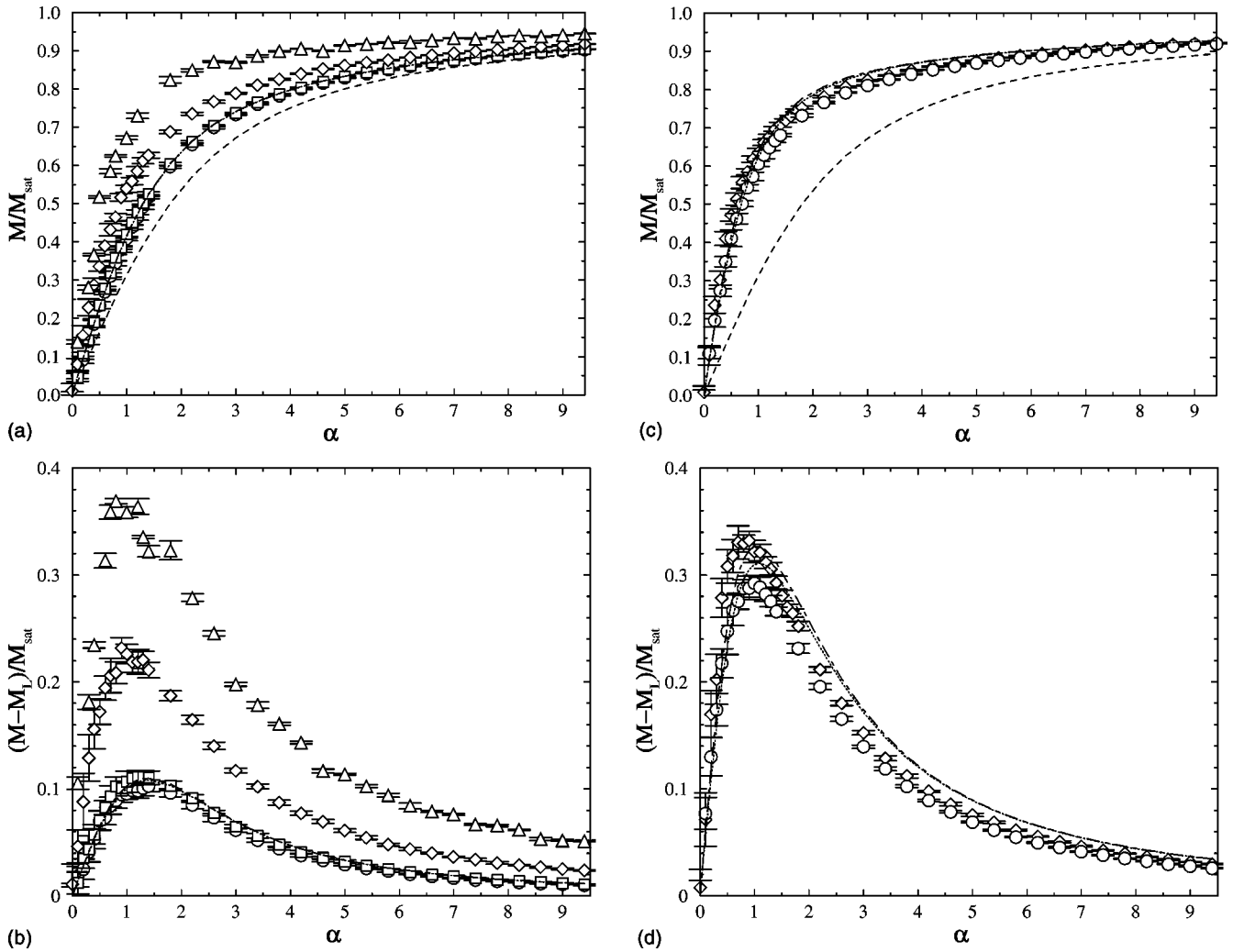

FIG. 3. Magnetization curves in the case of (a) $\chi_L=1.256$ for $\lambda=1$ (circles), 2 (squares), 4 (diamonds), and 8 (up-triangles); (c) $\chi_L=5.026$ for $\lambda=3$ (circles) and 4 (diamonds), respectively. The theoretical curves are given by the Langevin model [Eq. (1), dashed line], and by using Eq. (27) (dotted line) and Eq. (28) (dot-dashed line) in Eq. (26). The corresponding differences between the calculated magnetization and the Langevin model $(M-M_L)/M_{sat}$ are shown in (b) and (d), respectively.

of χ only at very small concentrations ($\phi<0.05$) for $\lambda>2$, but they dramatically overestimate the simulation results at larger values of ϕ.

Note that the simulations presented in Ref. [27] give rise to a susceptibility χ that *decreases* with growing λ if χ_L is fixed, which is *opposite* to our findings in Fig. 2(b). We suspect that this trend may be induced by finite size effects, since a *finite* spherical simulation volume with only a few 100 particles had been used in their simulations (without a periodic replication to properly account for the long-range dipolar interaction as is done in the present work). We shall clarify this point in a subsequent publication [31].

B. Magnetization curves

In this section, we extend the calculation of M to a larger range of the applied external field strength α in order to get the full magnetization curves. For moderately concentrated ferrofluids, the ''modified mean-field model'' [9] describes the magnetization curve in terms of the Langevin magnetization M_L [Eq. (1)] as follows:

$$M(H)=M_L(H_e), \tag{26}$$

where the effective field acting on an individual ferroparticle is given by

$$H_e=H+M_L(H)/3, \tag{27}$$

rather than $H_e=H+M/3$ as done in the Weiss model. The resulting expression for the initial susceptibility is Eq. (5). A higher-order description is obtained by replacing H_e in Eq. (27) by

$$H_e=H+\frac{M_L(H)}{3}+\frac{1}{144}M_L(H)\frac{dM_L(H)}{dH}, \tag{28}$$

which in the weak field limit reduces to Eq. (6) for χ [10]. The effective Langevin parameters corresponding to Eqs. (27) and (28) can be written as $\alpha_e=\alpha+\chi_L\mathcal{L}(\alpha)$ and $\alpha_e=\alpha+\chi_L\mathcal{L}(\alpha)+(\chi_L^2)/16\mathcal{L}(\alpha)(d\mathcal{L}(\alpha))/d\alpha$, respectively. This reflects the χ_L dependence of these two theoretical pre-

dictions. The Born-Mayer expansion described χ in a different way, where its dependence on ϕ and λ are given separately [11].

We investigated the magnetization curves for two different cases. In the first case χ_L is fixed to a small value of 1.256 where the predictions using Eqs. (27) and (28) practically coincide. Then λ is taken to be 1,2,4, and 8, respectively. To keep χ_L constant, the volume fraction ϕ had to be adapted from 0.157 down to 0.0196. In the second case, we take a larger value of $\chi_L = 5.026$ which makes the difference between the two theoretical predictions distinguishable by a few percentage. Only $\lambda = 3$ and 4 are discussed. The corresponding volume fractions are $\phi = 0.209$ and 0.157, respectively. In the latter case, we did not include the results for $\lambda \leqslant 2$ due to the limitation of the particle concentrations and for $\lambda = 8$ due to the extremely slow dynamics which prohibited us from reaching equilibrium distributions within our computational limits.

The calculated magnetization curves are shown in Figs. 3(a) and 3(c) together with the theoretical predictions using Eqs. (26–28). For a more explicit demonstration of the particle interaction, Figs. 3(b) and 3(d) display the difference between the simulation data and the Langevin model $(M - M_L)/M_{sat}$. The characteristic maximum of this difference is found to be at intermediate field strength of $\alpha \approx 1$, where it may reach more than 35%. The results in Figs. 3(a) and 3(b) reveal again the essential role of the dipolar coupling constant λ. When λ equals 1 and 2, the simulation and theoretical curves agree with each other very well. But for larger λ the calculated magnetization M rises with α much faster than the theoretical predictions, especially in the weak field regime. This reflects the same result already observed in Fig. 2, that χ increases with λ at low and moderate concentrations if χ_L is held fixed. Due to this effect, the peak positions of the increment $(M - M_L)/M_{sat}$ shift to smaller values of α with the increase of λ. In Figs. 3(c) and 3(d), the volume fraction of the particles are relatively high. The maximum absolute difference between the two analytical predictions occurs at $\alpha = 0.62$ where the result given by using Eq. (28) is about 4.3% larger than that by Eq. (27). Our simulation results are found to be consistent with both of them within the range of error bar. A quantitative analysis of the data indicates that Eq. (28) gives a better description in the weak field regime. This consequently leads to a better agreement between the simulation results on χ with the prediction of Eq. (6). However, both data sets for $\lambda = 3$ and $\lambda = 4$ show deviations from the theoretical curves at larger values of α which cannot be explained by statistical errors. Also here we infer that higher-order corrections are needed to more accurately describe the magnetization curves.

C. Microstructure analysis

The microstructure and its relation to the magnetic properties of ferrofluids are investigated by performing a cluster analysis. In conventional cluster analysis, agglomerates are usually defined on the base of the spatial proximity between the particles or by means of an energy criterion. For ferrofluids the latter one is more favorable, because the anisotropic dipolar interaction implies that two neighboring particles can form a stable bonding only if their dipole moments are roughly aligned in a head-to-tail orientation.

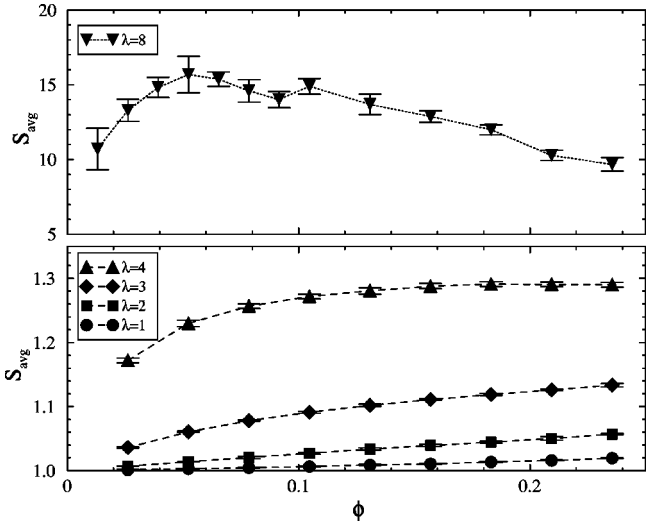

FIG. 4. Average size of the clusters formed at zero field as a function of λ and ϕ.

The energetically based cluster analysis of ferrofluids has been done in several different ways [14,16,21,27,35]. In this work, we adopt the definition of Refs. [14,16], and [21] where two particles are considered to be bound if their dipolar potential energy is less than a predetermined value U_{bond}. The influence of using different threshold values for U_{bond} has been investigated in a recent work [36]. The values of $-1.4\lambda kT$ [14,16] and $-1.5\lambda kT$ [21] were shown both to give good results. In our calculations we have varied U_{bond} from $-1.4\lambda kT$ to $-1.6\lambda kT$. Only slight quantitative changes of the results have been found without a qualitative difference. The results shown here have been evaluated for $U_{bond} = -1.5\lambda kT$, i.e., 75% of the contact energy of two perfectly coaligned dipolar particles. The above cluster definition implies that aggregates are mainly linear chains and rings. Thicker particle agglomerates or branched chains, however, occur very rarely in our simulations.

The size of a cluster is defined as the number of particles belonging to it. We first set up the connectivity matrix by means of our cluster definition, and then use it to evaluate the sizes and numbers of clusters in a given configuration. The average cluster size is defined by

$$S_{avg} = \left\langle \sum_s s n_s / \sum_s n_s \right\rangle, \tag{29}$$

where n_s is the number of clusters having size s, and the triangular brackets denote the time average or, equivalently, the average over the configuration space.

Figure 4 plots S_{avg} as a function of λ and ϕ for the case of zero field $(\alpha = 0)$. Clearly, increasing the dipolar coupling λ leads to a larger cluster size S_{avg}. However, in the weak coupling limit $\lambda = 1$ or 2, S_{avg} exceeds 1 only slightly, meaning that there are very few dimers present. Interparticle

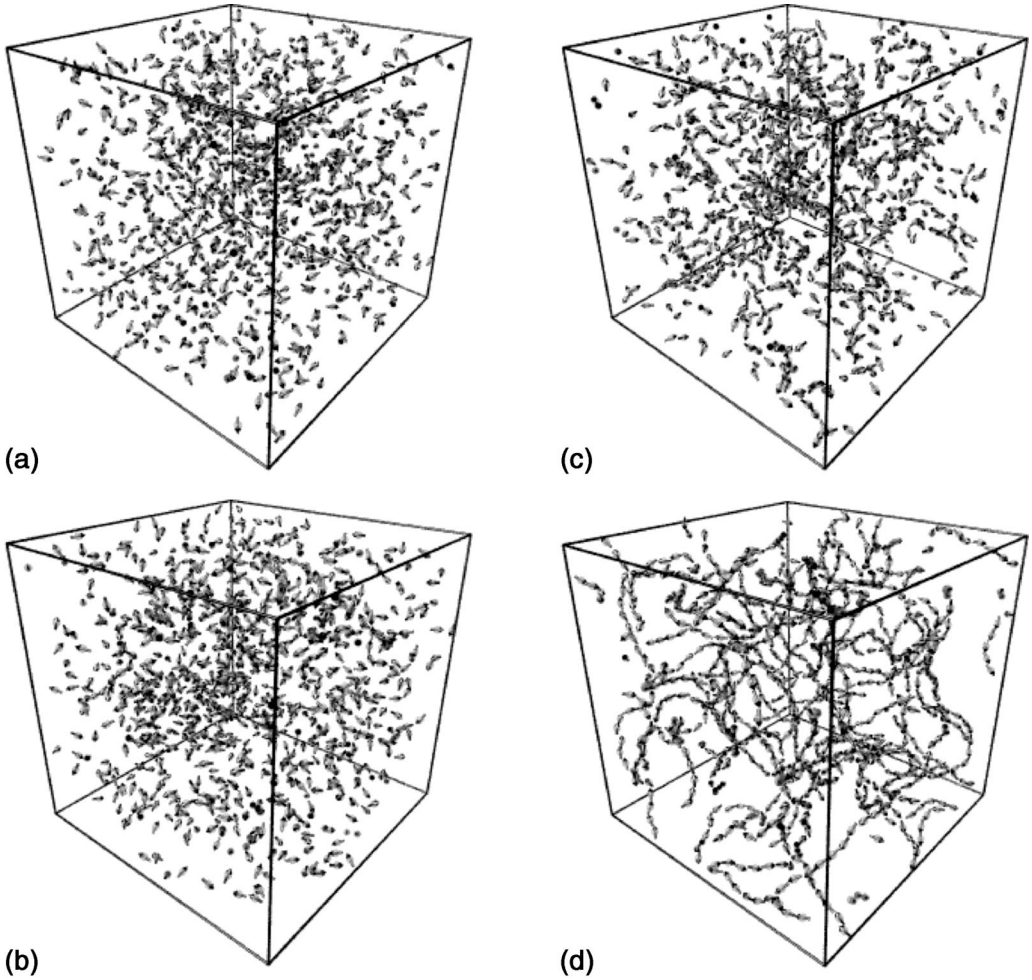

FIG. 5. Snapshot of the three-dimensional configurations formed at zero field in the systems of $\phi=0.052$ with $\lambda=1$ (a), 3 (b), 4 (c), and 8 (d), respectively. The arrows with length σ indicate the orientation of the dipole moments. The spheres (diameter$=\sigma/2$) show the center positions of the particles.

correlations seem to be weak and we already noted that the simulation results agree well with the theoretical models in these cases.

As λ is increased, the larger values of S_{avg} indicate the formation of more clusters. To elucidate this, we show snapshots of the three-dimensional configurations in Fig. 5 for the case of $\phi=0.052$ ($\rho^*=0.1$) at different λ values. The increase of the number and size of clusters with λ can be seen clearly in these figures. For $\lambda=3$ we find $S_{avg}=1.123$ at $\phi=0.052$. About 10% of the particles are organized in dimers and less than 1% in trimers. At the same density, S_{avg} increases to 1.481 for $\lambda=4$. Correspondingly, 22% of the particles are in dimers, 7% in trimers, and 2% in quadrumers. The density dependence of these numbers is shown in Fig. 6 where the average percentage of particles in n-mers are plotted as a function of ϕ for $\lambda=3$ and 4. It can be seen that more than 60% of the particles are still in monomers and the clusters with $s\geqslant 5$ are rarely found in these cases. However, when λ equals to 8, all the particles get involved in the formation of long chain-like structures. The average chain length is larger than 13σ at $\phi=0.052$. Due to thermal fluctuations, these chains are quite flexible. They are continuously breaking and recombining with others [14,16]. Even closed ring structures can be observed occasionally. In this strong coupling case, the chains have a close analogy to living polymers [16,36].

When the external field is switched on, the tendency of the dipole moments to coalign with the field direction enhances the aggregation probability. Accordingly the average cluster size is expected to increase with the field strength. Figure 7 shows the field-dependence of S_{avg} for the systems studied in Fig. 3(a). The increment of S_{avg} with α is only very weak for $\lambda\leqslant 2$, but it is more evident at $\lambda=4$. As exhibited in Fig. 8, the structure character of the system varies from randomly distributed short clusters to stringlike alignments along the magnetic flux with the increase of α. Consequently the cluster analysis in Fig. 9 reflects that more and more particles merge into larger aggregates. Cluster as long as $s=15$ could be observed at high α. But these stringlike structures in Fig. 8(d) are much more unstable than the chains formed at $\lambda=8$ [see Fig. 5(d)]. They posses a smaller contact energy so that thermal fluctuations can easily break long clusters into smaller segments. This effect is field independent. In fact, most of the strings observed in Fig. 8(d)

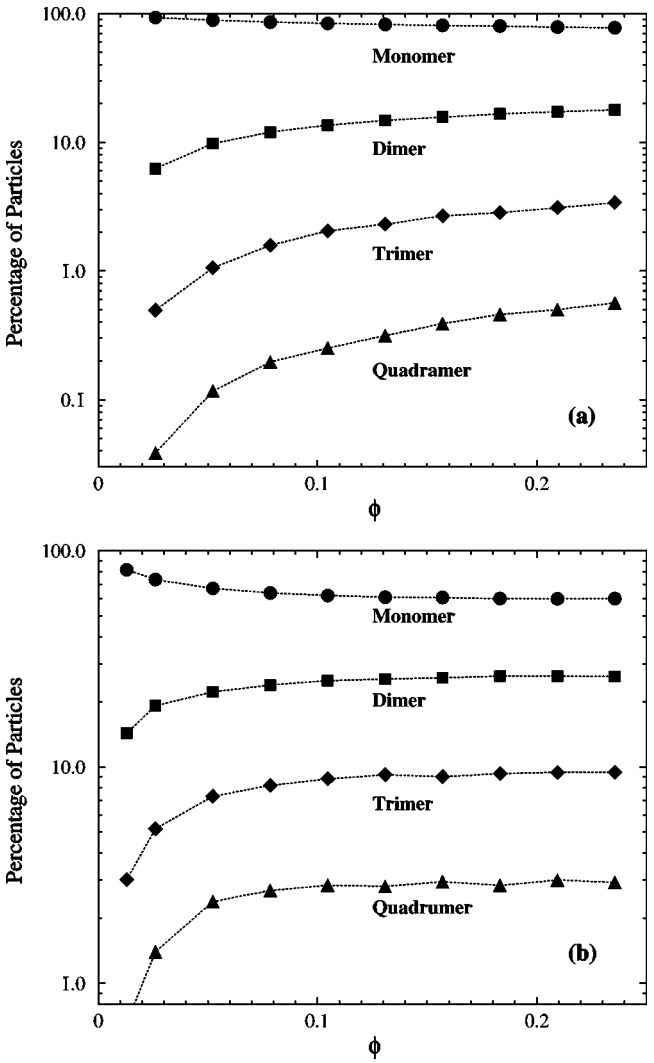

FIG. 6. Average percentage of the particles in *n*-mers for the system with $\lambda=3$ (a) and 4 (b) at zero field.

consist of a few continuously breaking and recombining segments. As a result, the average cluster size S_{avg} does not present a dramatic change as expected from the snapshot of the configurations. When $\lambda=8$, however, the long chains had already been formed even at zero field. The increase of the field strength just arranges these chains to have a better alignment along the field direction. But the average chain length does not change too much.

The results in Fig. 7 reveal that the magnetic field dependence of S_{avg} remains weak at small α. It is, therefore, legal to invoke the zero-field cluster analysis in order to interpret the outcomes related to the initial susceptibility (Fig. 2). Let us focus to the cases of $\lambda=3$ and 4 at low concentrations where the deviation between theory and simulation are most pronounced. In these cases the small clusters are relatively stable and spatially well separated from each other. For a rough approximation, we treat the clusters as rigid particles thus considering our system as a polydispersed sample. We define the effective dipole moment of each cluster according to

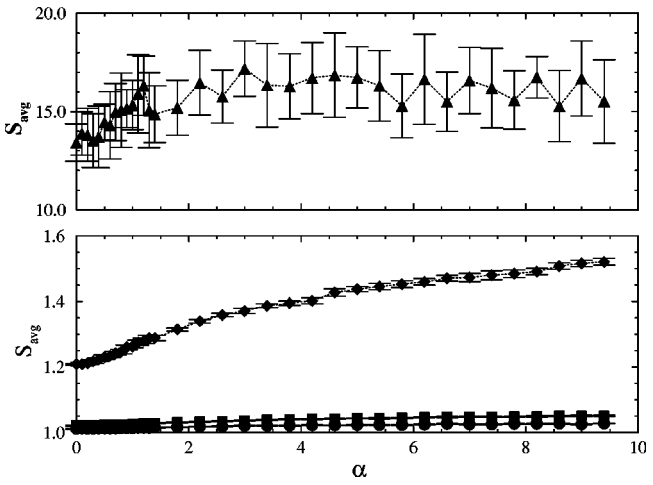

FIG. 7. Field dependence of the average cluster size of the systems studied in Fig. 3(a): $\lambda=1$ (circles), 2 (squares), 4 (diamonds), and 8 (up-triangles).

$$\mathbf{m}_s=\sum_{i=1}^{s}\mathbf{m}_i\,. \tag{30}$$

The effective Langevin susceptibility χ_L^{eff} of such a polydispersed system can be computed as

$$\chi_L^{eff}=\frac{1}{V}\frac{\left\langle \sum_{all\ clusters} m_s^2 \right\rangle}{3\mu_0 kT}. \tag{31}$$

Since most of the clusters are short linear *n*-mers, the value of χ_L^{eff} is larger than χ_L—the appropriate value for the monodispersed system. Replacing χ_L by χ_L^{eff} in Eq. (6) we get new modified theoretical curves. In Fig. 10 it can be seen that this simple operating prescription considerably improves the agreement between simulation and theory, at least at low concentrations. This proves that the formation of small clusters is responsible for the enhancement of the initial susceptibility.

At particle concentration above $\phi\simeq 0.1$, the modified theoretical curves start to overestimate the simulated χ values. In these cases, the increased angular correlations between the particles are not just limited to the two next nearest neighbors and thus make the above definition of clusters ambiguous [16]. Although we keep on using the energy criterion to obtain the cluster informations for Figs. 4 and 6, these values are more likely reflecting the local orientational order of the dipole moments. The clusters we find are not stable entities involving well-defined particle numbers as in the low density regime. This can be partially seen from the $S_{avg}(\phi)$ behavior in Fig. 4. When $\lambda\leqslant 2$, S_{avg} slightly increases with ϕ. But it saturates at $\lambda=4$ and even decreases at $\lambda=8$ for $\phi\geqslant 0.1$. Next, we examine the radial distribution function $g(r)$ of the system (Fig. 11), which gives the probability of finding a pair of particles a distance *r* apart, relative to the probability expected for a completely random distribution at the same density [29]. We find that the height of the first and second peaks, respectively, associated with dimer and trimers, de-

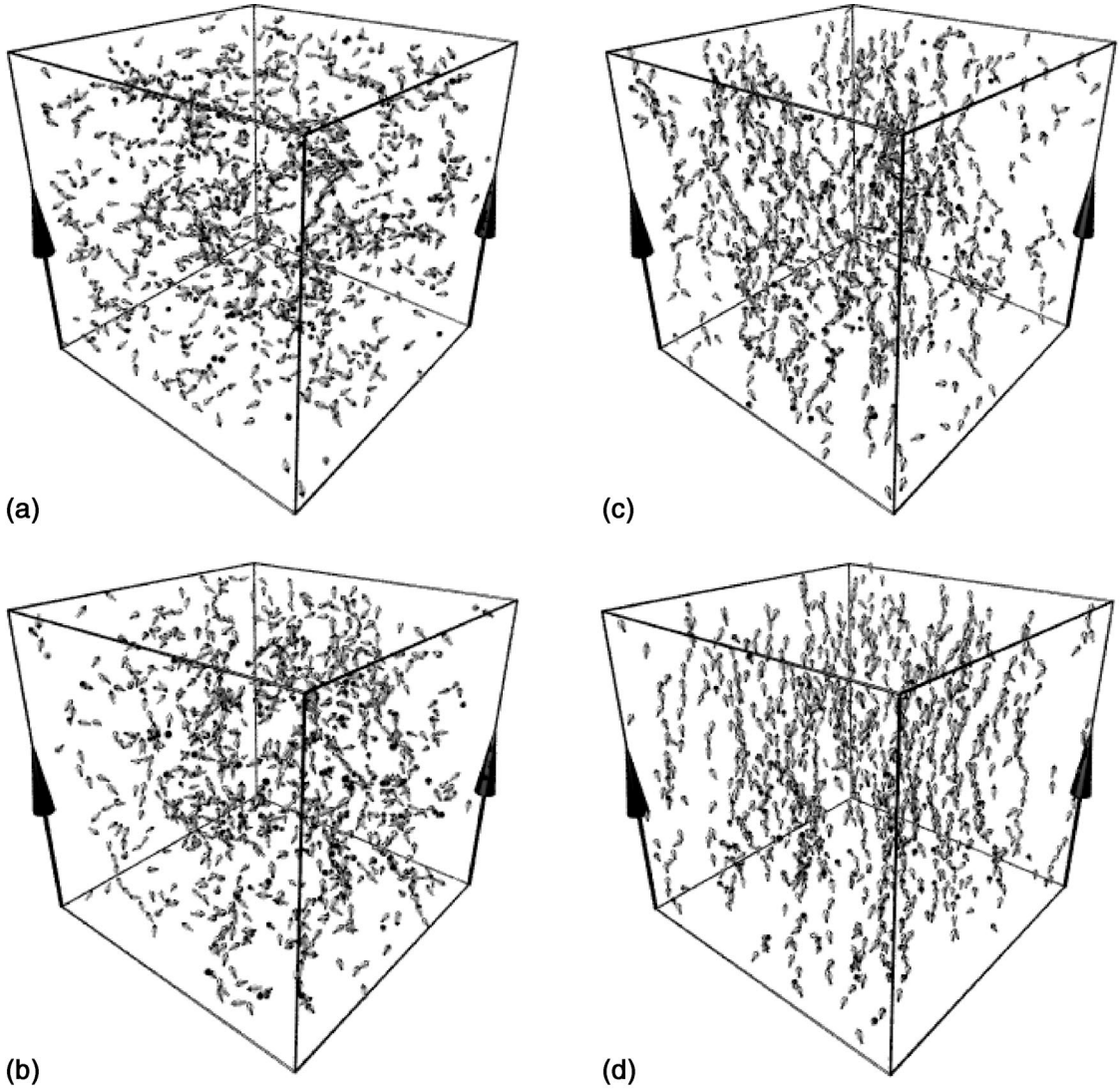

FIG. 8. Snapshot of the three-dimensional configurations formed in the system with $\phi = 0.0392$ and $\lambda = 4$ [studied in Fig. 3(a)] under the magnetic field of $\alpha = 0$ (a), 1.0 (b), 3.0 (c), and 9.0 (d), respectively. The arrows on the frame indicate the direction of the magnetic field.

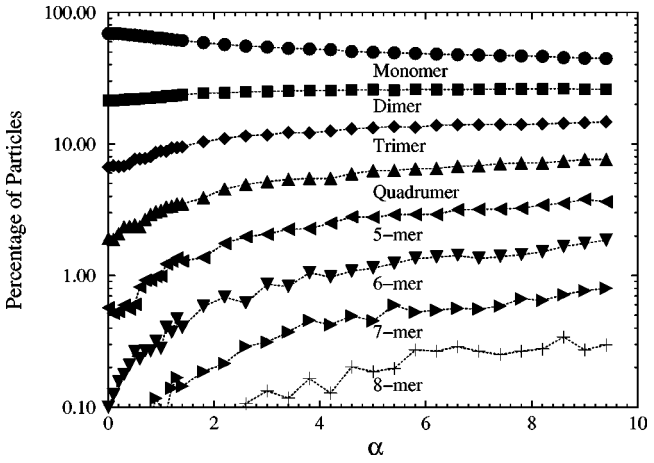

FIG. 9. Field dependence of the average percentage of particles in n mers for the system with $\phi = 0.0392$ and $\lambda = 4$.

crease with the increase of ϕ. This implies that the number of clusters does not increase as rapidly as the density [21]. In other words, upon raising ϕ the spatial distribution of the particle positions reapproaches to that of a homogeneous system. Therefore we expect our suggested modification with Eq. (31) only to be valid at low volume fractions below $\phi = 0.1$.

The formation of long chainlike structures in the strong coupling regime makes the systematic investigation of the magnetization properties at $\lambda = 8$ difficult. At $\phi = 0.0196$, there are very few overlaps between the elongated chains. They have enough free volume to rearrange in response to the external field. The magnetization of the system increases very fast in the weak field regime, as shown in Fig. 3(a). The occasional formation of a few closed ring structures is not found to affect noticeably the global magnetization behavior. On the other hand, when ϕ is enlarged, the chains become strongly entangled, like in a semiflexible polymer solution. This slows down the dynamics of the system dramatically. An extremely long simulation time is required to reach the

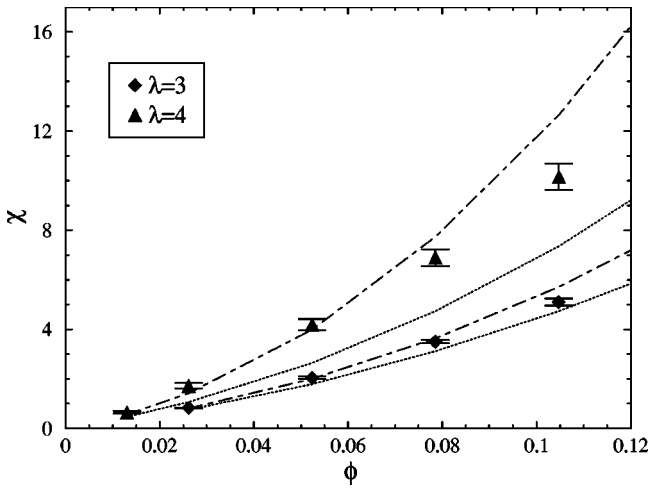

FIG. 10. Comparison of the simulation results on the initial susceptibility with the modified theoretical model. The curves are the theoretical prediction of Eq. (6) (dotted) and the modified theoretical results obtained by replacing χ_L with the effective Langevin susceptibility χ_L^{eff} in Eq. (6) (dot-dashed).

equilibrium state in the weak field regime. For example, at a density of $\phi=0.0785$, the equilibrium value of **M** at $\alpha=0.5$ is obtained only after 1.5 million simulation time steps. Simultaneously, since the number of particles is fixed in our simulation, the increase of ϕ makes the chain length become comparable to the size of the simulation box. This unavoidably induces finite size effects. For these reasons, we were unable to provide systematic investigations at $\lambda=8$ at higher concentrations (or equivalently larger χ_L), but only for $\chi_L=1.256$ shown in Fig. 3(a). These numerical difficulties could well be related to experimental observations which find a dramatic increase of viscosities at similar dipolar couplings [37].

D. Comparison with ferrosolids

To further investigate the influence of the cluster formation process we now turn to ferro-solid systems. By this we denote a suspension of dipolar particles which have their spatial positions frozen in, but are permitted to rotate freely. In this way the aggregation related effects in ferrofluids can easily be separated.

We prepared the initial configurations of the ferrosolid system by placing the particles randomly in the simulation box with random dipole moment orientations. For each given λ and ϕ, several different initial configurations were generated and simulated. They were found to give very similar results. Computer time limitations prohibited us to average over a large sequence of quenched configurations, which would be desirable to obtain a good ensemble average for a ferro-glass system. However, we have investigated this case only to study the qualitative influence of freezing the positional degrees of freedom. Accordingly, only the rotational equations of motion [Eq. (17)] of the particles need to be integrated in the simulations. Figure 12 displays the simulation results for the initial susceptibility at $\lambda=3$ and 4, along with the theoretical predictions for the fluid system. In ferrosolids χ also exhibits a nonlinear increase with the volume fraction ϕ. Comparing our data with the results of the ferrofluid system in Fig. 2, we see that the suppression of clusters leads to a slower increase of the magnetization at weak fields, and hence to a lower χ. It is interesting to note that the discrepancy between χ_{solid} and χ_{fluid} goes up when λ or ϕ are increased. This shows that the positional correlations are also very important at high density, and couple strongly to the dipolar rotational degrees of freedom, even if they do not evidently form stable clusters. A comparison of the phase behavior of the spatially frozen and fluid dipolar systems has also revealed the essential role of the positional correlations at high density [38,39]. Simulations showed that when the dipole moment has three components as studied in the present work, no long-range ferroelectric order exists in the randomly frozen systems at nonzero temperature. But the translational mobility of the particles in the fluid phase allows the build-up of the specific short-range correlations, and the system can be spontaneously polarized to develop a ferroelectric phase [18,19,38–40]. We consider the fact that the measured values of χ_{solid} coincide with the theoretical

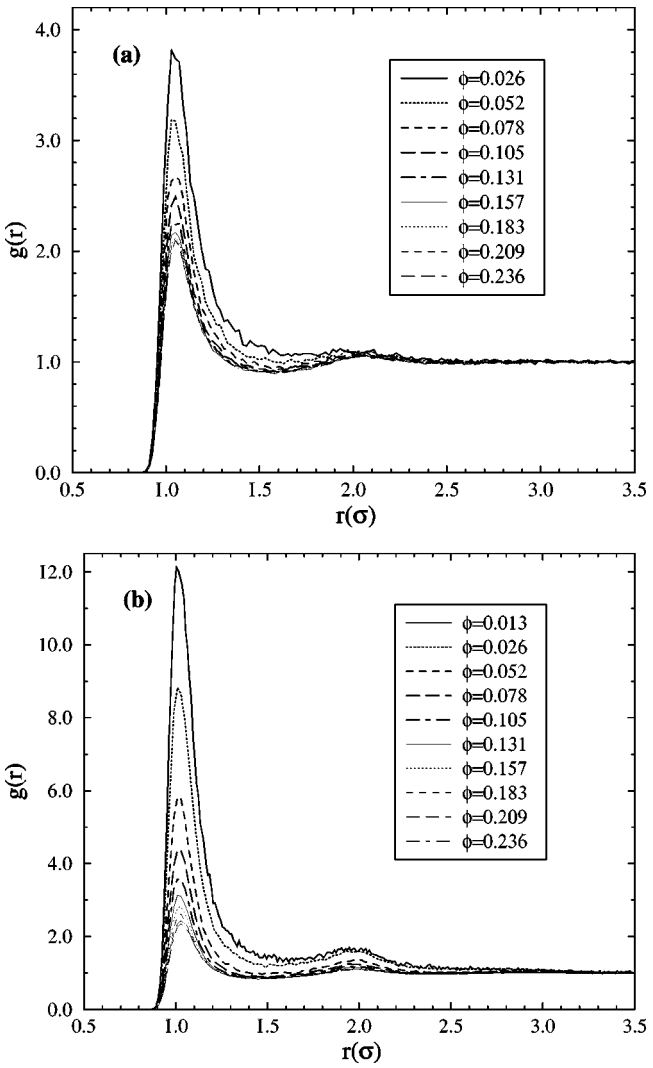

FIG. 11. Radial distribution function $g(r)$ for the cases of $\lambda=3$ (a) and 4 (b) as a function of ϕ at zero field.

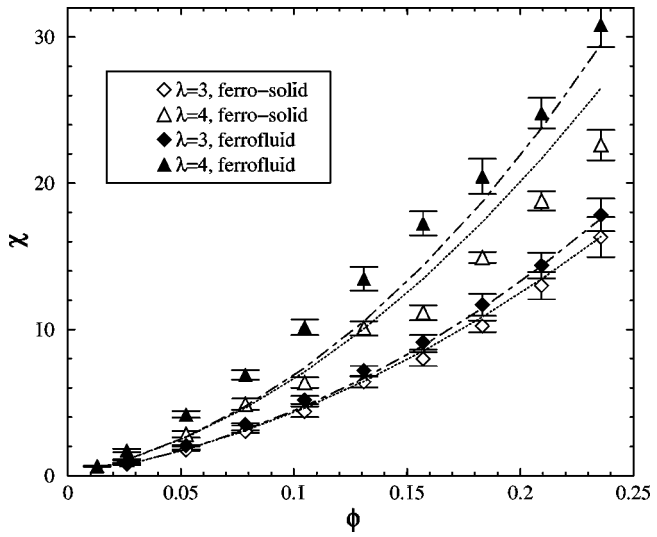

FIG. 12. Simulation results on the initial susceptibility of the ferro-solid systems with $\lambda=3$ and 4 as a function of the volume fraction ϕ and the dipolar coupling parameter λ. The analytical results on the ferrofluid system from Eq. (5) (dotted) and Eq. (6) (dot-dashed), as well as the simulation results from Fig. 2 are also included for comparison.

curves for the fluid system, Eqs. (5) and (6), almost exactly at low concentration for an accidental correspondence. At higher volume fractions the ferrosolid displays a susceptibility even below the theoretical prediction. This effect is more evident for larger λ at higher ϕ. Note, that in Ref. [27] a similar solidified ferrocolloid was investigated. There χ_{solid} was found to increase with χ_L, but the values are larger than that for the associated ferrofluid. Again we suspect that this is due to finite size effects of their sample.

We point out that the particles in our ferrosolid systems are supposed to be super-paramagnetic. This means that they have a negligible crystallographic magnetic anisotropy energy. There is no energy barrier which prevents the magnetic dipoles from a free rotation. That makes the present systems different from that studied in Ref. [26] where the initial susceptibility is found to decrease with the increase of the particle concentrations.

IV. CONCLUSION

We have investigated in detail the initial susceptibility, magnetization curve, and microstructure of ferrofluids in various particle concentration and dipolar coupling strength ranges by means of molecular dynamics simulations. The ferrofluid was modeled as a soft sphere system by means of a purely repulsive Lennard-Jones potential, and the magnetic cores interacting with a dipolar coupling strength λ from 1 to 8. The investigated volume fractions were in the range of $\phi \leqslant 0.24$ mostly. Our simulation method used the Ewald summation with metallic boundary conditions to deal with the long-range dipolar interactions, and took explicitly into account the translational and rotational degrees of freedom of the dipolar particles. The temperature was kept constant by means of a Langevin thermostat for all degrees of freedom. Our simulation results for the susceptibility show good agreement with the theoretical predictions in the weak coupling limit $\lambda \leqslant 2$. For higher dipolar couplings, however, we find systematic deviations from the theoretical predictions at low and intermediate concentrations. The detailed cluster analysis demonstrates that this is due to the particle aggregation at higher λ. The formation of clusters tend to increase the magnetization at weak field regime and consequently induce a larger initial susceptibility. At high densities, the spatial distribution of the particles starts to homogenize again, and the significance of clusters goes down. In fact we speculate that at higher concentrations there are almost no stable clusters any more, because they can disintegrate and reform with other particles rapidly. In this regime we find that the third-order equation in χ_L is compatible with our data.

For the magnetization curves we find that both, the second- and third-order theoretical curves, describe our data well for couplings $\lambda \leqslant 2$. For higher values of λ we find again systematic deviations. The system shows at coupling strength of $\lambda=8$ an almost gel-like behavior due to entangled chain structures. We expect this effect to become experimentally relevant in cobalt-based ferrofluids, where λ is large.

The influence of the aggregation phenomena was isolated by studying ferrosolids where the particles are randomly placed inside the simulation volume, and only rotations are allowed to occur. The observed initial susceptibilities are lower compared to the ferrofluid systems due to the suppression of cluster formation. The deviations to the fluid system grow with increasing dipolar coupling strength and increasing volume fraction.

ACKNOWLEDGMENTS

We thank B. Huke and S. Odenbach for helpful discussions. Financial support from the DFG under Grant No. HO 1108/8-2 is greatly appreciated.

[1] R.E. Rosensweig, *Ferrohydrodynamics* (Cambridge University Press, Cambridge, 1985).
[2] M.I. Shliomis, Usp. Fiz. Nauk **112**, 427 (1974) [Sov. Phys. Usp. **17**, 153 (1974)].
[3] A.F. Pshenichnikov, J. Magn. Magn. Mater. **145**, 319 (1995).
[4] L.J. Onsager, J. Am. Chem. Soc. **58**, 1486 (1936).
[5] K. O'Grady *et al.*, J. Magn. Magn. Mater. **31-34**, 958 (1983).
[6] M.S. Wertheim, J. Chem. Phys. **55**, 4291 (1971).
[7] K.I. Morozov and A.V. Lebedev, J. Magn. Magn. Mater. **85**, 51 (1990).
[8] Y.A. Buyevich and A.O. Ivanov, Physica A **190**, 276 (1992).
[9] A.F. Pshenichnikov, V.V. Mekhonoshin, and A.V. Lebedev, J. Magn. Magn. Mater. **161**, 94 (1996).
[10] A.O. Ivanov and O.B. Kuznetsova, Phys. Rev. E **64**, 041405 (2001).
[11] B. Huke and M. Lücke, Phys. Rev. E **62**, 6875 (2000).

[12] B. Groh and S. Dietrich, Phys. Rev. E **53**, 2509 (1996).
[13] B. Groh and S. Dietrich, Phys. Rev. E **57**, 4535 (1998).
[14] J.J. Weis and D. Levesque, Phys. Rev. Lett. **71**, 2729 (1993).
[15] J.J. Weis and D. Levesque, Phys. Rev. E **48**, 3728 (1993).
[16] D. Levesque and J.J. Weis, Phys. Rev. E **49**, 5131 (1994).
[17] P.J. Camp, J.C. Shelley, and G.N. Patey, Phys. Rev. Lett. **84**, 115 (2000).
[18] D. Wei and G.N. Patey, Phys. Rev. Lett. **68**, 2043 (1992).
[19] D. Wei and G.N. Patey, Phys. Rev. A **46**, 7783 (1992).
[20] M.J. Stevens and G.S. Grest, Phys. Rev. Lett. **72**, 3686 (1994).
[21] M.J. Stevens and G.S. Grest, Phys. Rev. E **51**, 5962 (1995).
[22] M.E. van Leeuwen and B. Smit, Phys. Rev. Lett. **71**, 3991 (1993).
[23] M.J. Stevens and G.S. Grest, Phys. Rev. E **51**, 5976 (1995).
[24] Y. Levin, Phys. Rev. Lett. **83**, 1159 (1999).
[25] T. Tlusty and S. Safran, Science **290**, 1328 (2000).
[26] R.W. Chantrell, N. Walmsley, J. Gore, and M. Maylin, Phys. Rev. B **63**, 024410 (2000).
[27] A.F. Pshenichnikov and V.V. Mekhonoshin, J. Magn. Magn. Mater. **213**, 357 (2000).
[28] S.W. de Leeuw, J.W. Perram, and E.R. Smith, Proc. R. Soc. London **373**, 27 (1980).
[29] M.P. Allen and D.J. Tildesley, *Computer Simulation of Liquids*, *Oxford Science Publications*, 1st ed. (Clarendon Press, Oxford, 1987).
[30] Z. Wang and C. Holm, J. Chem. Phys. **115**, 6351 (2001).
[31] Z. Wang, C. Holm, and H.W. Müller (unpublished).
[32] V.V. Murashov and G.N. Patey, J. Chem. Phys. **112**, 9828 (2000).
[33] P.G. Kusalik, J. Chem. Phys. **93**, 3520 (1990).
[34] W.H. Press, S.A. Teukolsky, W.T. Vetterling, and B.P. Flannery, *Numerical Recipes: The Art of Scientific Computing*, 2nd ed. (Cambridge University Press, Cambridge, 1992).
[35] G.N. Coverdale *et al.*, J. Magn. Magn. Mater. **188**, 41 (1998).
[36] J.M. Tavares, J.J. Weis, and M.M. TelodaGama, Phys. Rev. E **59**, 4388 (1999).
[37] S. Odenbach (private communication).
[38] G. Ayton, M.J.P. Gingras, and G.N. Patey, Phys. Rev. Lett. **75**, 2360 (1995).
[39] G. Ayton, M.J.P. Gingras, and G.N. Patey, Phys. Rev. E **56**, 562 (1997).
[40] J.J. Weis, D. Levesque, and G.J. Zarragoicoechea, Phys. Rev. Lett. **69**, 913 (1992).